AGU PUBLICATIONS

JGR

Journal of Geophysical Research: Solid Earth

RESEARCH ARTICLE
10.1002/2017JB014055

Key Points:
- The OH in dense silica decreases the transition pressure from rutile to $CaCl_2$ type and increases the pressure interval during the transition
- Dense hydrous silica phases are significantly more compressible than their anhydrous counterparts
- The direct substitution of $4H^+$ for Si^{4+} in the rutile-type hydrous phases would become energetically more stable with pressure

Supporting Information:
- Supporting Information S1

Correspondence to:
C. Nisr,
carole.nisr@gmail.com

Citation:
Nisr, C., K. Leinenweber, V. Prakapenka, C. Prescher, S. Tkachev, and S.-H. Dan Shim (2017), Phase transition and equation of state of dense hydrous silica up to 63 GPa, *J. Geophys. Res. Solid Earth*, *122*, 6972–6983, doi:10.1002/2017JB014055.

Received 1 FEB 2017
Accepted 22 JUN 2017
Accepted article online 1 AUG 2017
Published online 9 SEP 2017
Corrected 26 OCT 2017

This article was corrected on 26 OCT 2017. See the end of the full text for details.

Phase transition and equation of state of dense hydrous silica up to 63 GPa

C. Nisr[1], K. Leinenweber[2], V. Prakapenka[3], C. Prescher[3,4], S. Tkachev[3], and S.-H. Dan Shim[1]

[1]School of Earth and Space Exploration, Arizona State University, Tempe, Arizona, USA, [2]Department of Chemistry and Biochemistry, Arizona State University, Tempe, Arizona, USA, [3]Center for Advanced Radiation Sources, University of Chicago, Chicago, Illinois, USA, [4]Now at Institute of Geology and Mineralogy, University of Cologne, Cologne, Germany

Abstract Although it has previously been considered to be essentially anhydrous, Al-free stishovite can contain up to ~1.3 wt % of H_2O, perhaps through the direct substitution ($Si^{4+} \rightarrow 4H^+$), according to recent studies. Yet the stability of such substitution and its impact on the properties of silica and rutile-structured hydrous phases (such as δ-AlOOH and phase H) are unknown at the conditions of the deeper mantle. We have synthesized hydrous and anhydrous Al-free stishovite samples at 723 K and 9 GPa, and 1473 K and 10 GPa, respectively. Synchrotron X-ray diffraction patterns show that the unit cell volume of hydrous stishovite is 1.3% greater than that of anhydrous stishovite at 1 bar, suggesting significant incorporation of OH in the crystal structure (3.2 ± 0.5 wt % H_2O). At 300 K, we found a lower and broader transition pressure from rutile type to $CaCl_2$ type (28–42 GPa) in hydrous dense silica. We also found that hydrous silica polymorphs are more compressible than their anhydrous counterparts. After the phase transition, the unit cell volume of hydrous silica becomes the same as that of anhydrous silica, showing that the proton incorporation through a direct substitution can be further stabilized at high pressure. The lower pressure transition and the pressure stabilization of the proton incorporation in silica would provide ways to transport and store water in the lower mantle in silica-rich heterogeneities, such as subducted oceanic crust.

1. Introduction

Silica (SiO_2) is an archetypical material for the silicate mineralogy of Earth and terrestrial planets. Up to 9 GPa, crystal structures of all pure silica polymorphs are built from SiO_4 tetrahedra. At higher pressures, stishovite, a denser SiO_2 polymorph, is stable in a rutile-type structure ($P4_2/mmn$) with octahedrally coordinated Si [*Stishov and Popova*, 1961]. Stishovite undergoes a displacive second-order phase transition to the orthorhombic $CaCl_2$-type structure (*Pnnm*) at ~50 GPa [*Kingma et al.*, 1995; *Andrault et al.*, 1998, 2003].

Below 300 km depth in the mantle, stishovite is expected to exist in the silica-rich parts of subducting slabs (such as sediments and basaltic crust) [*Irifune and Ringwood*, 1993]. High-pressure experiments have shown that the content of stishovite increases with pressure in the mid-oceanic ridge basalt composition as the phase relation changes, reaching ~20 vol % at the shallow lower mantle [*Ricolleau et al.*, 2010; *Hirose et al.*, 2005; *Grocholski et al.*, 2013]. Its presence in the deep Earth has been also demonstrated through diamond inclusions [*Walter et al.*, 2011].

Although stishovite has been considered to be a nominally anhydrous mineral [*Bell and Rossman*, 1992], it can contain 72–2900 ppm of water in conjunction with Al incorporation [*Pawley et al.*, 1993; *Chung and Kagi*, 2002; *Litasov et al.*, 2007]. On the other hand, much lower water content has been reported for Al-free stishovite (~100 ppm H_2O) [*Pawley et al.*, 1993]. From these observations, it has been thought that water is incorporated into the crystal structure of stishovite through a charge coupled substitution ($Si^{4+} \rightarrow Al^{3+} + H^+$). However, the amount of hydrogen in these samples is not nearly equal to the amount of Al. Instead, it can only compensate for up to 40% of the introduced Al^{3+} [*Pawley et al.*, 1993; *Bolfan-Casanova et al.*, 2000; *Bromiley et al.*, 2006; *Litasov et al.*, 2007]. These observations are difficult to explain unless there exist other substitution mechanisms in addition to the charge-coupled substitution for water incorporation.

Spektor et al. [2011] have shown that the quantities of water on the percent level can be incorporated into otherwise pure SiO_2 at 9–10 GPa and at low temperature. They suggested that $4H^+$ substitute directly for Si^{4+}

in the octahedral site. The solubility reported in *Spektor et al.* [2011] exceeds the solubility previously reported for Al-free stishovite [*Pawley et al.*, 1993; *Bromiley et al.*, 2006; *Bolfan-Casanova et al.*, 2000; *Litasov et al.*, 2007] by a factor of 500 or more.

The presence of Al and/or H can alter the transition pressure from stishovite to the $CaCl_2$ type. *Bolfan-Casanova et al.* [2009] have found that anhydrous Al-bearing stishovite undergoes a phase transition to the $CaCl_2$-type structure at 23 GPa and 300 K. *Lakshtanov et al.* [2007] reported that the incorporation of 6.1 wt % Al_2O_3 and 0.24 t % H_2O into silica also reduces significantly the transition pressure to 20–24 GPa at 300 K . From the low-pressure phase transition in dry aluminous stishovite at 23 GPa, *Bolfan-Casanova et al.* [2009] suggested that it is Al that promotes the lowering in the phase transition pressure.

Recent high-pressure experiments have discovered rutile-structured (or its modified versions) hydrous phases stable at the pressure-temperature conditions related to the mantle, such as phase H, δ-AlOOH, and their potential solid solutions [*Ohtani et al.*, 2014; *Nishi et al.*, 2014; *Ohira et al.*, 2014]. These phases have been considered as favorable candidates for water storage in the deep lower mantle. The rutile-type structures and their lower symmetry phases can be hydrated through multiple different substitution mechanisms, including the coupled substitution (Al^{3+} + H^+ for Si^{4+}) and direct substitution ($4H^+$ for Si^{4+}). Therefore, studying water-rich Al-free stishovite allows us to isolate the effects of the direct substitution on the phase transition and the physical properties in the rutile-type phases at the high-pressure conditions of the Earth's interior.

2. Experimental Methods

We have synthesized water-rich Al-free stishovite in a 6–8 multianvil press using a 14/8 assembly [*Leinenweber et al.*, 2012] at Arizona State University. The silica glass starting material with 1 μm grain size (SPEX, purity 99.999%) was loaded into a silver capsule together with H_2O. The capsule was sealed by pressure crimping. We synthesized the sample at 9 GPa and 450°C for 49 h (Table 1). Excess H_2O was found after the experiment, indicating that silica was exposed to free H_2O throughout the synthesis (further information on the synthesis method can be found in *Nisr et al.* [2017]). Optical observation indicated a grain size of ~1 μm. For an internally consistent comparison with the water-rich stishovite sample, we also synthesized a pure SiO_2 stishovite phase without water at 10 GPa and 1200°C (Table 1).

We loaded separate cold-pressed foils of the water-rich and anhydrous stishovite samples together in the same sample chamber of a diamond-anvil cell (DAC). The sample chamber was made by drilling a 120 or 260 μm diameter hole in a rhenium gasket indented by diamond anvils with either 200 or 400 μm diameter culet, respectively. We added a piece of Au foil in the sample chamber next to both samples which served as a pressure calibrant [*Fei et al.*, 2007]. We loaded helium as a pressure-transmitting medium using the gas-loading system at GeoSoilEnviroConsortium for Advanced Radiation Sources (GSECARS) [*Rivers et al.*, 2008].

We have performed in situ synchrotron X-ray diffraction (XRD) at the GSECARS sector of the Advanced Photon Source using a MarCCD detector. We have collected data at room temperature for both water-rich and anhydrous stishovite samples using a monochromatic X-ray beam with a wavelength of 0.3344 Å and a beamsize of $3 \times 4\ \mu m^2$. For one of the three runs we present here, a membrane push plate was attached to the DAC in order to adjust the pressure with a precision of ~0.5 to 1 GPa. We compressed the samples up to ~63 GPa, while we collected diffraction patterns every 3 to 5 GPa during compression on three different spots: on water-rich stishovite, on anhydrous stishovite, and on the Au foil.

We have integrated the diffraction images to 1-D diffraction patterns using the DIOPTAS software [*Prescher and Prakapenka*, 2015]. Using LaB_6 standard, we corrected the distortions and the detector distance (~200 mm) from the data. We have determined the pressure from the unit cell volume of Au obtained by fitting individual peaks using the equation of state of Au of *Fei et al.* [2007]. We have then performed Rietveld refinement on the diffraction patterns using the general structure analysis program package, GSAS [*Larson and Von Dreele*, 1988]. During Rietveld refinement, we have refined the unit cell parameters, the preferred orientation function, the peak profile shape function, and the scale factors. Due to the resolution limit, we did not refine the atomic positions. The residual after background subtraction ($R_{wp-bknd}$) of our refined diffraction patterns ranges between 5 and 7%.

We have also conducted Raman measurements on the hydrous stishovite sample at 1 bar and 300 K (Figure 1), in order to confirm the incorporation of structural OH in the sample. For the Raman excitation source, we used the 532 nm beam from a frequency doubled Nd:YAG laser. The power at the surface of the sample was 30 mW.

Table 1. Synthesis Conditions for the Water-Rich and Anhydrous Stishovite Samples in the Multianvil Press

	Loading (mg)		Synthesis				
	SiO_2	H_2O	P (GPa)	T (°C)	Duration (h)	Capsule	Composition
Hydrous	7.6	4.2	9	450	49	Ag	$Si_{0.954}O_2H_{0.184}$
Anhydrous	23.6	0	10	1200	1	Pt	SiO_2

The spectrometer was calibrated using the neon emission spectral lines. The spectra for the starting stishovite sample were collected for a few minutes. We report the interpretation of the 1 bar spectra and high-pressure spectra of the sample in *Nisr et al.* [2017].

3. Results

3.1. OH in the Sample

Although the diffraction patterns of water-rich stishovite are similar to anhydrous stishovite at 1 bar, we found that the diffraction peaks of the water-rich sample are all systematically shifted to lower 2θ angles compared to anhydrous stishovite. The observation suggests that the incorporation of proton increases the length of the unit cell axis and, therefore the unit cell volume, of stishovite (Table 2). Our Raman measurements on this sample confirmed the existence of the structural OH from the observation of the OH stretching modes (Figure 1).

Spektor et al. [2011] previously reported the relationship between the water content and the unit cell volume of hydrous stishovite phases with a water content ranging from 0.5 to 3 wt %. The 3 wt % they found is in the sample synthesized at 10 GPa and 400°C [*Spektor et al.*, 2016] that resulted in a mixture of two phases, one less hydrous and one more hydrous. The maximum amount they found in their synthesized single-phase samples was 1.3 wt % and corresponds to a sample synthesized at ~10 GPa and 450°C.

Our sample synthesized at 9 GPa and 450°C contains 3.2 ± 0.5 wt % water based on the relationships from *Nisr et al.* [2017]. The calibration reported in *Nisr et al.* [2017] was conducted using the data in *Spektor et al.* [2011, 2016] (additional information on the determination of the water content can be found in the supporting information). Considering the errors from the synthesis pressure and temperature determination for our sample and *Spektor et al.* [2011] sample, the water content we found is in the same order of magnitude of that of *Spektor et al.* [2011] and is much higher than the water content previously reported in Al-free stishovite (72 ppm) [*Bolfan-Casanova et al.*, 2000] and in Al-bearing stishovite (82–2900 ppm) [*Pawley et al.*, 1993; *Chung and Kagi*, 2002; *Panero et al.*, 2003; *Litasov et al.*, 2007]. In addition, because Raman is much less sensitive to

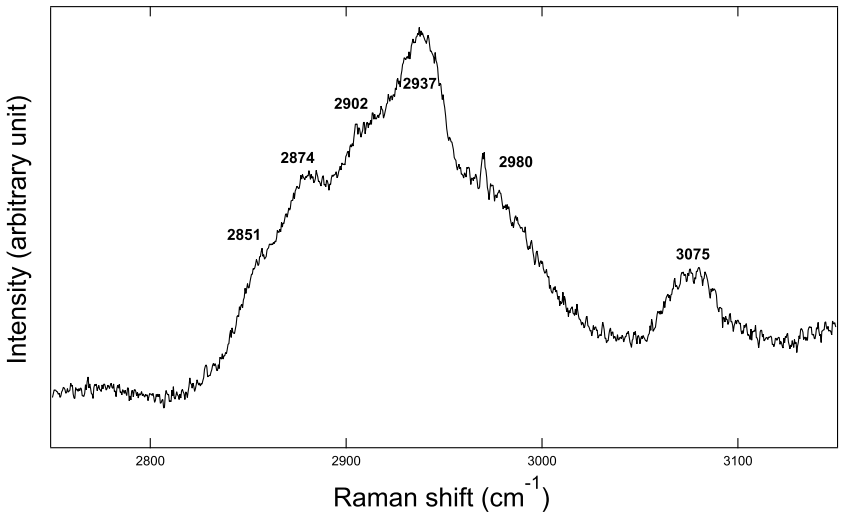

Figure 1. Raman spectrum of water-rich stishovite at the OH stretching region at 1 Bar and 300 K.

Table 2. Unit Cell Parameters of the Water-Rich and Anhydrous Stishovite Samples at 1 Bar and 300 K[a]

	a (Å)	c (Å)	V_0 (Å^3)	Water Content (wt %)
Hydrous	4.2068(9)	2.6669(9)	47.198(21)	3.2(5)
Anhydrous	4.1805(9)	2.6647(9)	46.569(11)	0

[a]The water content of hydrous stishovite is estimated from the calibration presented in *Nisr et al.* [2017] which is updated from the calibration used in *Spektor et al.* [2011]. If we use the calibration by *Spektor et al.* [2011], we obtain 2.7 wt % for the water content.

OH than IR and normally limited to water contents higher than 0.1 – 1 wt % for the detection, the intense OH modes we detected in our Raman measurements (Figure 1) are qualitatively consistent with the estimated amount of water.

3.2. Phase Transition

Our water-rich stishovite sample shows broad diffraction peaks which make the detection of subtle peak splitting challenging. However, we found that some diffraction lines, 101, 210, and 301, show changes in pressure-induced shift in the *d* spacings starting from ~28 GPa, suggesting possible peak splittings by a phase transition. Furthermore, our Raman study at high pressure detected much more clear changes in both lattice and OH modes at ~24 GPa [*Nisr et al.*, 2017]. Therefore, we conducted series of Rietveld refinements with different approaches.

We first attempted Rietveld refinement with a starting model including only a single phase of rutile-type crystal structure. Although the changes we found in the diffraction patterns are much more subtle compared with the Raman spectra, we found that tetragonal symmetry of stishovite does not provide sufficient quality fitting to the observed diffraction peak positions at pressures higher than 28 GPa. For example, as shown in Figure 2a, the stishovite structure cannot fit significant intensity at the higher angle side of the 101 peak. The stishovite structure also fails to explain the observed peak position of 200. It is also clear that the stishovite structure cannot correctly predict the observed peak position of 210 from sinusoidal shaped fit residue. Such systematic misfits are clear indications of changes in the crystal structure with subtle nature within our resolution.

We have therefore conducted Rietveld refinements on each diffraction pattern above 25 GPa using two additional starting models: a two-phase model with the rutile (tetragonal) and $CaCl_2$-type (orthorhombic) phases and a single-phase model with the $CaCl_2$ type. Between 28 and 42 GPa, Rietveld refinements with the two-phase model decrease $R_{wp-bknd}$ (fit residue after background subtraction) significantly (by ~23%) over the single phase model with the $CaCl_2$ type (Figure 2). This difference in $R_{wp-bknd}$ remains almost the same until 42 GPa, where the single-phase model with $CaCl_2$ type starts to show a better $R_{wp-bknd}$ than the two-phase model (higher by ~4%), indicating that the phase transformation of water-rich stishovite was completed. This is clear in Figure 3 which displays the same diffraction pattern of the water-rich phase at 47.6 GPa and 300 K, refined as a two-phase model with the rutile and $CaCl_2$-type phases (Figure 3a), and as a single-phase model with the $CaCl_2$-type structure (Figure 3b). The pattern analyzed as a $CaCl_2$-type structure shows a better refinement at 2θ angles of 10 – 12° and 14 – 17°, where significant mismatches were observed for the 120 + 210 and 031 + 301 lines. At this pressure, the sample is fully in the high-pressure structure with an orthorhombic unit cell. We have also identified new phonon lines and changes in the frequency shifts at 24 – 28 GPa in our recent high-pressure Raman measurements on the same sample [*Nisr et al.*, 2017]. The spectral changes we identified there are also consistent with a phase transition.

Although we tentatively used the crystal structure of the $CaCl_2$ type in this study, there are other structures which are also related to the rutile-type structure and can also explain the lower symmetry indicated by our diffraction patterns. For example, δ-AlOOH has a modified rutile-type structure ($Pmn2_1$) and an orthorhombic unit cell [*Suzuki et al.*, 2000; *Komatsu et al.*, 2006]. Both $CaCl_2$-type and δ-AlOOH structures yield the same fitting to lattice parameters because the Si-O sublattices are isosymmetric. The space group difference between them is mainly due to the existence and the location of the hydrogen atoms in the δ-AlOOH structure: in δ-AlOOH there is a cross bonding of hydrogen between second-neighbor AlO_6 octahedra. Because of the small X-ray scattering cross section of the hydrogen atom, XRD patterns would look essentially the same for these two possibilities. Therefore, it is sufficient to use the $CaCl_2$-type structure for fitting the XRD patterns of the lower symmetry hydrous silica structure we found at pressures higher than ~25 GPa in this study.

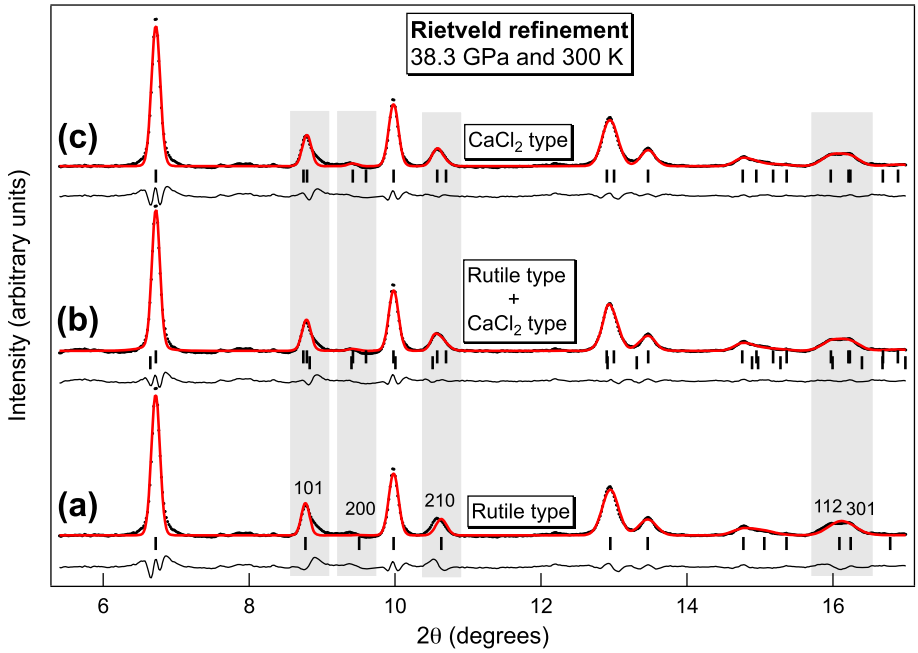

Figure 2. Rietveld refinement results for the diffraction patterns at 38.3 GPa and 300 K using three different starting models: (a) a single-phase model with the rutile-type phase, $R_{wp-bknd} = 6.8\%$, (b) a two-phase model with the rutile and $CaCl_2$-type phases, $R_{wp-bknd} = 5.2\%$, and (c) a single-phase model with the $CaCl_2$-type phase, $R_{wp-bknd} = 6.8\%$. The black points are the measured diffraction intensities, the solid red lines are the calculated intensities, and the black lines below the patterns are the difference between the observed and calculated intensities. The upper and lower tick marks in the middle pattern indicate diffraction peak positions of the $CaCl_2$-type and stishovite phases, respectively. The tick marks in Figures 2a and 2c are for the rutile and the $CaCl_2$-type phases, respectively. The grey rectangles highlight the difference in fitting using single-phase models and a two-phase model. The backgrounds of the diffraction patterns were subtracted.

3.3. Unit Cell Parameters and Equation of State

We compare the unit cell parameters of water-rich silica with those of anhydrous silica and δ-AlOOH in Figure 4. We note that our anhydrous dense silica sample was measured in the same sample chamber in the DAC, providing internally consistent comparison between hydrous and dry counterparts. Our anhydrous stishovite c/a ratio is in agreement with the result of *Andrault et al.* [2003].

At 1 bar, the proton incorporation into the crystal structure of stishovite increases its a axis while the c axis does not change significantly. This observation is in agreement with *Spektor et al.* [2011, 2016]. The high-pressure behavior of the c axis is almost indistinguishable between water-rich and anhydrous silica (Figure 4a). Therefore, the differences shown in Figure 4b for the c/a ratio of water-rich dense silica and anhydrous dense silica are mostly from the changes in the a axis. At low pressures, anhydrous stishovite and water-rich stishovite show similar increasing trend of the c/a ratio. The rate of increase in c/a decreases with pressure in both anhydrous and water-rich stishovite at about ~60 GPa and ~25 GPa, respectively, where both undergo the phase transition from the rutile type to the $CaCl_2$ type. The pressure where the sign changes in the slope in anhydrous stishovite coincides with the phase transition pressure from the rutile type to $CaCl_2$ type. If we apply the same criteria to our water-rich stishovite, we can estimate the transition pressure to be ~25–40 GPa, supporting our assignment of a phase transition being similar to anhydrous stishovite but at much lower pressure.

At the phase transition, two identical tetragonal a axes of the rutile-type structure separate into orthorhombic a and b axes (Figure 4b). In our 3.2 wt % water bearing SiO_2, the stishovite to the $CaCl_2$-type transition can be located where diverging trends of the two different axial ratios at 28 GPa and 300 K start in Figure 4b. As discussed above, the XRD patterns indicate coexistence of both low- and high-pressure phases in water-rich dense silica for a pressure range of about 14 GPa. At 42 GPa, the phase transition completes within the resolution of our XRD. Again, this confirms our assignment that the tetragonal to orthorhombic transition found

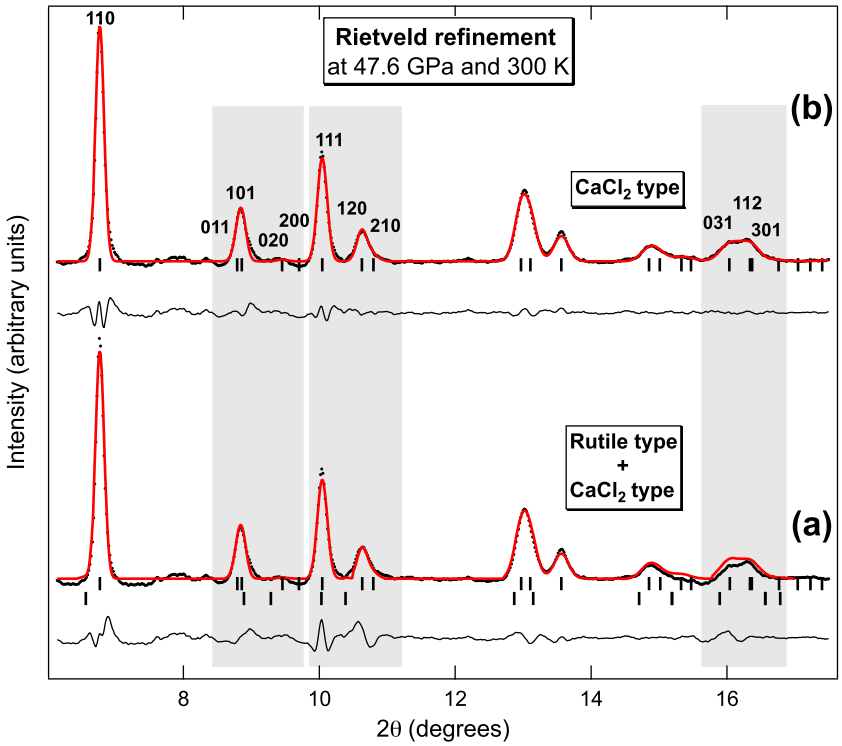

Figure 3. Rietveld refinements of a diffraction pattern at 47.6 GPa and 300 K. (a) The pattern is refined with a two-phase model where both rutile and $CaCl_2$-type phases are included ($R_{wp-bknd}$ = 7.2%). (b) We show a fitting result for the same diffraction pattern but with a single-phase $CaCl_2$-type model ($R_{wp-bknd}$ = 6%). The black points are the data, the solid red lines are the calculated patterns, and the black lines below the patterns are the difference. The upper and lower tick marks in the bottom pattern indicate diffraction peak positions of the $CaCl_2$-type and stishovite phases, respectively. The tick marks in Figure 3b are for the $CaCl_2$-type phase. The grey rectangles highlight the improvements in the difference in fitting in both structural models. The backgrounds of the diffraction patterns were subtracted.

in 3.2 wt % hydrous SiO_2 is significantly lower than the similar phase transition in anhydrous SiO_2 at 50 GPa [*Kingma et al.*, 1995]. Therefore, OH severely affects the phase behavior of silica.

For the $CaCl_2$-type phases in both water-rich and aluminous systems, the axial ratio changes with pressure. Near 60 GPa, c/a for both water-rich and aluminous dense silica seems to have a similar magnitude as anhydrous dense silica phase in the $CaCl_2$-type structure. Also, c/a and c/b for both water-rich and aluminous dense silica in the $CaCl_2$-type diverge rapidly after the transition pressure. From these similar behaviors we can interpret that H and Al facilitate the distortion of the $CaCl_2$-type structure similarly between the transition pressure and 60 GPa. While the c/b of aluminous dense silica appears similar to that of anhydrous dense silica, the c/b of water-rich pure dense silica is lower than both anhydrous pure dense silica and aluminous dense silica. The smaller c/b indicates a higher degree of relative expansion in the b direction in hydrous $CaCl_2$-type phase through the direct substitution ($Si^{4+} \rightarrow 4H^+$) of proton. Although H or Al seem to have the same effect on the structure of stishovite by lowering the transition pressure, the effect of H_2O on the transition pressure and distortion is much stronger than that of Al_2O_3 in terms of the number of Si replaced, as evident from the difference in the c/b ratio between water-rich and aluminous $CaCl_2$-type phases at high pressures. Therefore, Figure 4 indicates that Al and H should affect the structure differently through different substitution mechanisms.

Under the conditions studied, the axial ratios do not come close to the distortions present in δ-AlOOH nor does the a axis show a high degree of compression that might be expected from hydrogen bonding along the a axis in that structure. We can therefore hypothesize that the bulk of the behavior observed is characteristic of the isolated and noninteracting H_4O_6 groups.

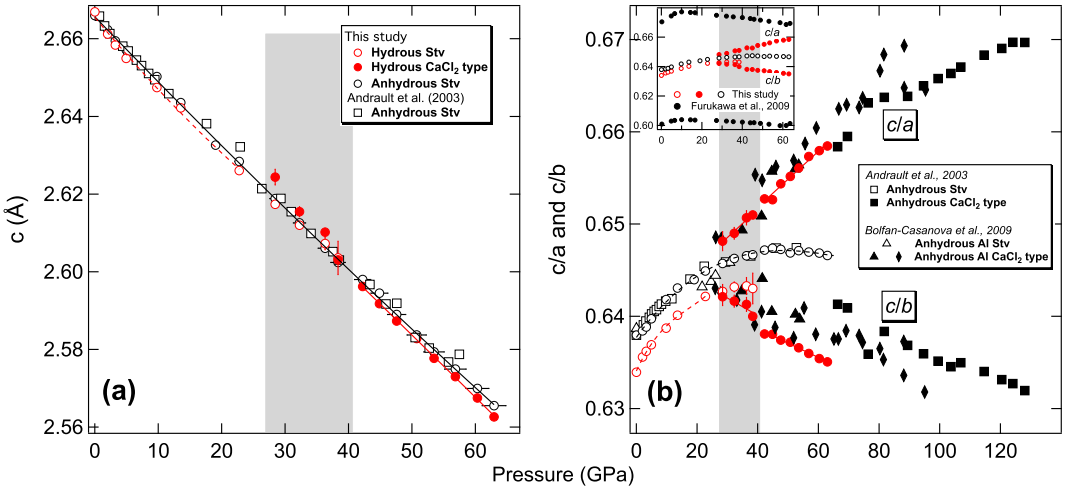

Figure 4. The (a) c axis and (b) c/a and c/b ratios of silica as a function of pressure. Open symbols are for the rutile structure, and closed symbols are for the $CaCl_2$-type structure. Triangles and diamonds are for two different runs of anhydrous aluminous SiO_2 from *Bolfan-Casanova et al.* [2009] (AlSti-5 and PV20, respectively). Error bars represent 1σ uncertainties. The grey indicates the pressure range where the rutile and $CaCl_2$-type phases coexist in our study. The inset in Figure 4b shows the c/a and c/b ratios of δ-AlOOH [*Sano-Furukawa et al.*, 2009] in comparison with the hydrous SiO_2 data in this study.

We compare the unit cell volumes of dry and water-rich stishovite samples measured in the same sample chamber of the diamond-anvil cell under quasi-hydrostatic stress conditions in a He medium. At pressures between 0 and ~40 GPa, the water-rich silica phase has a larger unit cell volume than the anhydrous phase due to the expansion of the unit cell by the proton incorporation (Figure 5). After the complete transition to the $CaCl_2$ type at 42 GPa, the unit cell volume of water-rich dense silica becomes the same as the unit cell volume of anhydrous stishovite, and with pressure, it starts to become even smaller.

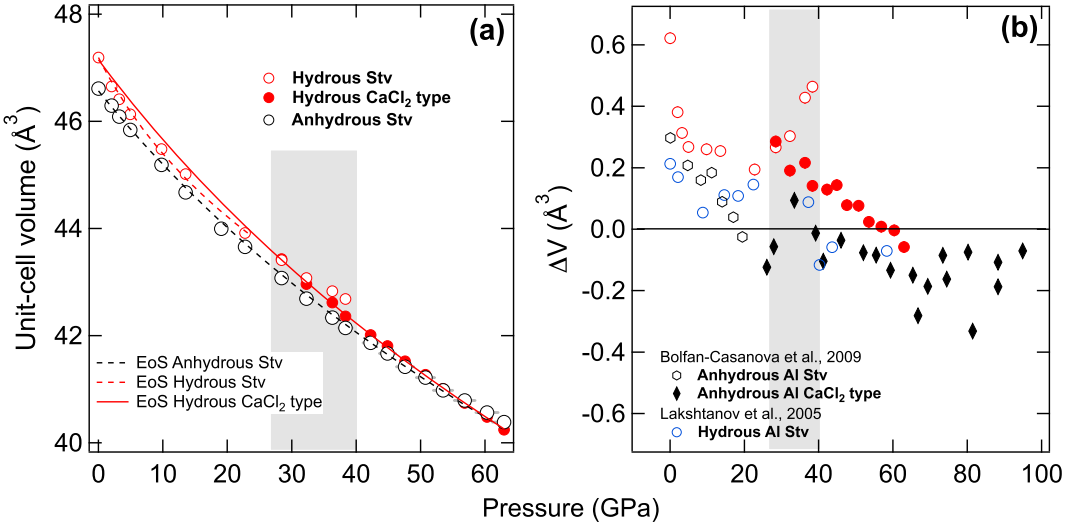

Figure 5. (a) The unit cell volume of anhydrous and hydrous silica samples at 300 K as a function of pressure. The black dashed, red dashed, and red solid lines represent the results of the least squares fitting to Birch-Murnagham EOS for anhydrous stishovite, water-rich stishovite, and water-rich dense silica in $CaCl_2$-type structure, respectively. (b) The difference in unit cell volume compared with anhydrous pure silica (solid line). For comparison, we also show data from other studies on different compositions: anhydrous Al silica [*Bolfan-Casanova et al.*, 2009] and hydrous Al silica [*Lakshtanov et al.*, 2005]. In Figure 5b, hexagons and diamonds are two different runs of anhydrous Al silica from *Bolfan-Casanova et al.* [2009] (AlSti-1 and PV20, respectively). In all our data, errors in volumes measurements are smaller than the size of the symbols. The grey areas indicate the pressure range where both rutile and $CaCl_2$ type exist together. The volume and lattice parameters of our anhydrous and hydrous silica at each pressure can be found in the supporting information.

Table 3. Equation of State of the Stishovite Phases[a]

K_0 (GPa)	K_0'	V_0 (Å^3)	References
		Anhydrous Stishovite	
312(2)	4.59[b]	46.569[b]	This study
310(1)	4.59(23)	46.51(61)[c]	*Andrault et al.* [2003]
		Hydrous Stishovite	
257(9)	4.59[b]	47.191[b]	This study
		Aluminous Stishovite	
292(7)	4.59[b]	46.77(13)[c]	*Bolfan-Casanova et al.* [2009]
		Aluminous Hydrous Stishovite	
304(3)	4.00[b]	46.782(10)[c]	*Lakshtanov et al.* [2005]

[a]The numbers in the parenthesis are the estimated 1σ uncertainties.
[b]Fixed during EOS fit.
[c]Measured value and fixed during EOS fit.

We have fit the refined unit cell volumes of anhydrous stishovite, water-rich stishovite, and water-rich $CaCl_2$-type phase at different pressures to the Birch-Murnagham equation of state [*Birch*, 1978]. The fit for anhydrous stishovite up to ~64 GPa yielded $K_0 = 312 \pm 2$ GPa (K_0: bulk modulus) for $V_0 = 46.569$ Å^3 (V_0: unit cell volume at 1 bar) and $K_0' = 4.59$ (K_0': pressure derivative of K_0). We fixed V_0 to the measured value at 1 bar and K_0' for the value from *Andrault et al.* [2003]. The K_0 value for anhydrous stishovite is consistent with the result by *Andrault et al.* [2003] (Table 3).

We have fit the data of water-rich stishovite up to ~23 GPa, and we have obtained $K_0 = 257 \pm 9$ GPa with K_0' fixed to 4.59 (same as the anhydrous stishovite) and with V_0 fixed to the measured volume (47.191 Å^3) (Table 3). For water-rich silica in the $CaCl_2$-type structure, we fit the unit cell volumes at 42–63 GPa for K_0' fixed to 4. Because the high-pressure phase is not quenchable and therefore V_0 is unknown, we also fit for V_0. The fitting yielded $K_0 = 286 \pm 18$ GPa and $V_0 = 47.23 \pm 0.36$ Å^3 (Table 4). Although the fitted V_0 of the $CaCl_2$-type phase is slightly higher than that of water-rich stishovite, it is indistinguishable from the water-rich stishovite within the estimated uncertainty.

Andrault et al. [2003] found $K_0 = 334 \pm 7$ GPa with $K_0 = 4$ and $V_0 = 46.31$ Å^3 for anhydrous $CaCl_2$-type phase. It is clear that water-rich dense silica phases are significantly more compressible than their anhydrous counterparts. The smaller bulk moduli we found for the water-rich dense silica phases likely result from the presence of H that softens hydrous silica phases and from the presence of Si vacancies. Because of its higher compressibility, the unit cell volume of hydrous $CaCl_2$ tends to converge to anhydrous $CaCl_2$-type phase at high pressures. However, although the water-rich phase is more compressible than the anhydrous phase for the $CaCl_2$ type, it is still less compressible than the water-rich stishovite.

Table 4. Equation of State of the $CaCl_2$-Type Phases[a]

K_0 (GPa)	K_0'	V_0 (Å^3)	References
		Anhydrous $CaCl_2$ Type	
334(7)	4.00	46.31[b]	*Andrault et al.* [2003]
		Hydrous $CaCl_2$ Type	
286(18)	4.00[b]	47.23(36)	This study
		Aluminous $CaCl_2$ Type	
322(7)	4.00[b]	45.51(13)	*Bolfan-Casanova et al.* [2009]

[a]The numbers in the parenthesis are the estimated 1σ uncertainties.
[b]Fixed during EOS fit.

4. Discussion and Conclusions

4.1. Energetics of the Proton Incorporation in the Rutile-Type Dense Hydrous Phases

Water can be stored in the nominally anhydrous minerals at elevated temperatures in the mantle [*Bolfan-Casanova et al.*, 2000]. In particular, the major phases, such as wadsleyite and ringwoodite in the mantle transition zone, can store large amounts of structurally bound water [*Bell and Rossman*, 1992; *Smyth et al.*, 1995; *Rossman*, 1996; *Hirschmann*, 2006]. However, it has been shown that the main constituents of the lower mantle have a very little water solubility [*Bolfan-Casanova et al.*, 2000, 2003; *Panero et al.*, 2003, 2015], leading to a view in which the lower mantle is dry [*Hirschmann*, 2006; *Karato*, 2011].

Recent discovery of hydrous phases stable at the pressure-temperature conditions related to the mantle such as phase H and δ-AlOOH has open-up possibilities to store water in the deep mantle [*Ohtani et al.*, 2014; *Nishi et al.*, 2014]. Because of their complex chemical compositions in the multicomponent systems [*Ohtani et al.*, 2014], some number of different substitution mechanisms should exist for the water incorporation in these phases in the mantle. These hydrous phases have rutile-type or modified versions of the structures, and therefore, our results on hydrous stishovite provide insights on the energetics of the direct substitution ($4H^+$ for Si^{4+}) and on the impact of the substitution to the physical properties of the hydrous phases.

Because of the very high pressure in the region, the reactions in the lower mantle are often dominated by pressure effects (or toward more densely packed crystal structures) [*Ito et al.*, 1990]. In order to gain insights for the energetics of the direct substitution ($Si^{4+} \rightarrow 4H^+$) at mantle-related pressures, we compared the unit cell volumes of the hydrous and anhydrous dense silica phases (stishovite and $CaCl_2$ type) we measured (Figure 5). At lower pressures, the molar volume of hydrous stishovite is already smaller than the volume of stishovite + H_2O [*Spektor et al.*, 2011]. According to our results, once hydrous stishovite is transformed, the unit cell volume of the hydrous $CaCl_2$-type silica rapidly approaches to that of the anhydrous dense silica. Eventually, the unit cell volume of hydrous silica could become indistinguishable from the anhydrous silica at ~50 GPa. The fact that the ΔV for hydrous silica has a negative slope (Figure 5b) means that the compressibility of hydrous $CaCl_2$ type is greater, making the proton incorporation through the direct substitution even more stabilized at the higher-pressure conditions of the deeper mantle.

In order to understand the effects of the compression on the Al charge coupled substitution, we also plotted the unit cell volumes of anhydrous aluminous dense silica phases (black diamonds and open hexagons) [*Bolfan-Casanova et al.*, 2009] together with the unit cell volume of hydrous aluminous stishovite (blue circles) [*Lakshtanov et al.*, 2005] in Figure 5b. We found some difficulties, however, in the Al case. Although *Bolfan-Casanova et al.* [2009] used a single composition (4 wt % Al_2O_3) for the starting material, they found after synthesis a range of different unit cell volumes for the recovered samples at 1 bar, indicating a range of different Al incorporation in their dry silica samples (2.2–3.6 wt % Al_2O_3). Furthermore, the volume data they presented are not consistent with each other due possibly to the different Al incorporation, annealing, and synthesis conditions (therefore, we distinguish these different runs in Figures 4 and 5).

Despite the difference in Al content (1.8 wt %), the data points for hydrous aluminous stishovite by *Lakshtanov et al.* [2005] agree well with the data points for anhydrous aluminous stishovite by *Bolfan-Casanova et al.* [2009]. Therefore, in hydrous aluminous case (or the Al charge coupled substitution), Al has the dominant effects on the unit cell volume of stishovite. If indeed Al continues to be the main factor for reducing ΔV, although direct data do not exist, the Al silica data by *Bolfan-Casanova et al.* [2009] may suggest further stabilization of the Al charge coupled substitution in the stability field of the $CaCl_2$-type phase (Figure 5). Therefore, through this comparison, we can conclude that both the direct substitution and the Al charge coupled substitution can become more stable with pressure, resulting in an enhanced volume stabilization from the proton incorporation in the deep mantle. It is compelling that the decreasing trends in ΔV found in Figure 5b may indicate potentially an increasing water solubility in silica and even in the hydrous phases with structures related to the rutile type and $CaCl_2$ type, such as phase H and δ-AlOOH with depth (or pressure). It will be important for the future studies to measure the unit cell volumes of a wide range of compositions particularly at pressures higher than 60 GPa. Also, it is important to conduct direct hydrothermal synthesis of the dense silica phases (in particular, the $CaCl_2$ type) to further explore the intriguing possibility for larger water storage in the deeper mantle.

It is of interest to know which of the two possible proton substitution mechanisms is more stable: the Al charge coupled substitution or the direct substitution. While hydrous aluminous stishovite (blue circles [*Lakshtanov et al.*, 2005] (Figure 5b); Al charge coupled substitution) appears to have a slightly lower unit cell volume than

pure hydrous stishovite (red circles; direct substitution), from the data scatter, it is difficult to be conclusive. More importantly, volume data do not exist for hydrous Al silica in the $CaCl_2$ type. In addition, a disproportionally large amount of Al compared with proton in the hydrous Al sample plotted in the figure (1.8 wt % Al_2O_3 and 500 ppm water) suggests that the data reflect more about the effect of the defect involved substitution ($Si^{4+} + 1/2O^{2-} \rightarrow Al^{3+} + 1/2V_O$, where V_O is oxygen vacancy) rather than the Al charge coupled substitution ($Si^{4+} \rightarrow Al^{3+} + H^+$). Therefore, it remains unclear which one of the two substitutions is energetically more favorable. Instead, it is perhaps more reasonable to think that the two substitutions are both energetically competitive and therefore exist in the rutile-type and $CaCl_2$-type phases in the lower mantle.

In this study, we also showed that dense silica experiences a large decrease in the bulk modulus by hydration through the direct substitution. Due to the paucity of data, it is less clear if the hydration through the Al charge substitution can have the same impact, particularly in the deeper mantle. It is of interest if the hydration of stishovite can also affect other physical properties, such as the viscosity and the strength. The mechanical properties are of particular interest as they may affect whether the oceanic crust can be detached from the subducting slabs or not deeper in the mantle.

4.2. Effects of the Proton Incorporation on the Phase Transitions in Dense Silica

Some seismic structures have been documented at depths between 800 and 1900 km in the lower mantle [*Kawakatsu and Niu*, 1994; *Le Stunff et al.*, 1995; *Niu et al.*, 2003]. Because stishovite undergoes a phase transition to the $CaCl_2$ type at pressure conditions similar to those expected for the depth [*Kingma et al.*, 1995; *Andrault et al.*, 1998, 2003], the possible relationship between the seismic observation and the stishovite transition has been discussed [*Vinnik et al.*, 2001]. Because free silica may not exist in the bulk lower mantle, such possibility should be explored in the context of Si-rich heterogeneities, such as subducting oceanic crust, which can have a sufficient amount of silica for the seismic observation of the phase transition [*Ricolleau et al.*, 2010; *Hirose et al.*, 2005; *Grocholski et al.*, 2013].

Lakshtanov et al. [2007] found a much lower transition pressure (20–24 GPa) at 300 K in silica with 6.1 wt % Al_2O_3 and 0.24 wt % H_2O. Furthermore, Al alone can decrease the phase transition pressure significantly [*Bolfan-Casanova et al.*, 2009]. However, it remains uncertain which of the Al or the H can influence the transition pressure more significantly. For example, *Umemoto et al.* [2016] showed through first-principles calculation that the protons in aluminous hydrous stishovite are more important in lowering the transition pressure. What appears to be more robust is that the magnitude of the pressure decrease is sensitive to the amounts of Al_2O_3 and water in silica [*Lakshtanov et al.*, 2005, 2007; *Bolfan-Casanova et al.*, 2009].

In this study, we have found that proton alone can decrease the pressure of the phase transition from stishovite to $CaCl_2$-type phase by ~25 GPa. The magnitude is similar to the case of hydrous aluminous stishovite [*Lakshtanov et al.*, 2007]. Yet because the substitution mechanism expected for our pure dense silica is different from aluminous silica, our observation does not necessarily mean that proton plays a more important role than Al in hydrous aluminous silica. Because we studied only one composition, the relationship between the concentration of proton and the phase transition remains unknown. Therefore, it is important for future studies to measure the effect of different proton contents on the stishovite to $CaCl_2$-type phase transition.

Our Raman measurements also show a series of changes between 24 and 28 GPa for the same sample [*Nisr et al.*, 2017]. The transition pressure and the interval are, however, not the same as our XRD measurements reported here, 28–42 GPa. The comparison of the pressure interval for the transition should be made with care because there are many experimental factors which can affect the differences, such as differences in the pressure medium (Ar for Raman and He for XRD), the data coverage (no diffraction patterns between 22 and 28 GPa), and the resolution. In particular, in our hydrous samples, the diffraction peaks are broader and therefore subtle peak splitting is difficult to detect.

However, it is clear from both Raman and XRD that the stishovite to $CaCl_2$-type transition occurs over a finite pressure interval in our water-rich stishovite. This is an unexpected behavior compared with pure anhydrous stishovite since the transition is displacive and therefore does not have a pressure interval where both low- and high-pressure phases exist together [*Kingma et al.*, 1995; *Andrault et al.*, 1998]. It is possible that the incorporation of protons increases the kinetic barrier of the phase transition. Through first-principles calculations, *Umemoto et al.* [2016] suggested that the incorporation of protons can change the nature of the transition to a first-order phase transition in hydrous aluminous silica. Because the proton dynamic during the phase

transition plays a key role for the change, despite the fact that the calculation was conducted for hydrous aluminous silica, a similar explanation may be applicable for our pure hydrous silica. This change in the nature of the phase transition should be considered in applying the laboratory measurements on the physical property changes across the phase boundary to seismic studies, as the property changes [*Carpenter et al.*, 2000; *Shieh et al.*, 2002] should be sensitive to whether the transition remains second order (in anhydrous stishovite) or changes to first order (in hydrous stishovite).

Acknowledgments
We thank two anonymous reviewers and the Editor for the helpful discussions. This work has been supported by an NSF grant to K.L., S.H.S., and C.N. (EAR1321976). The results reported herein also benefited from collaborations and/or information exchange within NASA's Nexus for Exoplanet System Science (NExSS) research coordination network sponsored by NASA's Science Mission Directorate. Portions of this work were performed at GSECARS (University of Chicago, Sector 13). GSECARS is supported by the NSF (EAR-1128799) and DOE (DE-FG02-94ER14466). APS is U.S. DOE Office of Science User Facilities operated for the DOE Office of Science by ANL (DE-AC02-06CH11357). The use of the COMPRES-GSECARS gas loading system was supported by COMPRES (NSFEAR-11-57758) and by GSECARS (NSFEAR-1128799 and DOEDE-FG02-94ER14466). All of our data are presented in the supporting information.

References

Andrault, D., G. Fiquet, F. Guyot, and M. Hanfland (1998), Pressure-induced Landau-type transition in stishovite, *Science*, *282*(5389), 720–724.
Andrault, D., R. J. Angel, J. L. Mosenfelder, and T. L. Bihan (2003), Equation of state of stishovite to lower mantle pressures, *Am. Mineral.*, *88*(2–3), 301–307.
Bell, D. R., and G. R. Rossman (1992), Water in Earth's mantle: The role of nominally anhydrous minerals, *Science*, *255*(5050), 1391–1397.
Birch, F. (1978), Finite strain isotherm and velocities for single-crystal and polycrystalline NaCl at high pressures and 300 K, *J. Geophys. Res.*, *83*(B3), 1257–1268.
Bolfan-Casanova, N., H. Keppler, and D. C. Rubie (2000), Water partitioning between nominally anhydrous minerals in the MgO-SiO_2-H_2O system up to 24 GPa: Implications for the distribution of water in the Earth's mantle, *Earth Planet. Sci. Lett.*, *182*(3), 209–221.
Bolfan-Casanova, N., H. Keppler, and D. C. Rubie (2003), Water partitioning at 660 km depth and evidence for very low water solubility in magnesium silicate perovskite, *Geophys. Res. Lett.*, *30*(17), 1905, doi:10.1029/2003GL017182.
Bolfan-Casanova, N., D. Andrault, E. Amiguet, and N. Guignot (2009), Equation of state and post-stishovite transformation of Al-bearing silica up to 100 GPa and 3000 K, *Phys. Earth Planet. Inter.*, *174*(1), 70–77.
Bromiley, G. D., F. A. Bromiley, and D. W. Bromiley (2006), On the mechanisms for H and Al incorporation in stishovite, *Phys. Chem. Miner.*, *33*(8–9), 613–621.
Carpenter, M. A., R. J. Hemley, and H.-k. Mao (2000), High-pressure elasticity of stishovite and the reversible $P4_2/mnm$ to $Pnnm$ phase transition, *J. Geophys. Res.*, *105*, 10,807–10,816.
Chung, J. I., and H. Kagi (2002), High concentration of water in stishovite in the MORB system, *Geophys. Res. Lett.*, *29*(21), 2020, doi:10.1029/2002GL015579.
Fei, Y., A. Ricolleau, M. Frank, K. Mibe, G. Shen, and V. Prakapenka (2007), Toward an internally consistent pressure scale, *Proc. Natl. Acad. Sci. U.S.A.*, *104*(22), 9182–9186.
Grocholski, B., S.-H. Shim, and V. Prakapenka (2013), Stability, metastability, and elastic properties of a dense silica polymorph, seifertite, *J. Geophys. Res. Solid Earth*, *118*, 4745–4757, doi:10.1002/jgrb.50360.
Hirose, K., N. Takafuji, N. Sata, and Y. Ohishi (2005), Phase transition and density of subducted MORB crust in the lower mantle, *Earth Planet. Sci. Lett.*, *237*(1), 239–251.
Hirschmann, M. M. (2006), Water, melting, and the deep Earth H_2O cycle, *Annu. Rev. Earth Planet. Sci.*, *34*, 629–653.
Irifune, T., and A. Ringwood (1993), Phase transformations in subducted oceanic crust and buoyancy relationships at depths of 600–800 km in the mantle, *Earth Planet. Sci. Lett.*, *117*(1–2), 101–110.
Ito, E., M. Akaogi, L. Topor, and A. Navrotsky (1990), Negative pressure-temperature slopes for reactions forming $MgSiO_3$ perovskite from calorimetry, *Science*, *249*(4974), 1275–1279.
Karato, S.-I. (2011), Water distribution across the mantle transition zone and its implications for global material circulation, *Earth Planet. Sci. Lett.*, *301*(3), 413–423.
Kawakatsu, H., and F. Niu (1994), Seismic evidence for a 920-km discontinuity in the mantle, *Nature*, *371*(6495), 301–305.
Kingma, K. J., R. E. Cohen, R. J. Hemley, and H.-k. Mao (1995), Transformation of stishovite to a denser phase at lower-mantle pressures, *Nature*, *374*(6519), 243–245.
Komatsu, K., T. Kuribayashi, A. Sano, E. Ohtani, and Y. Kudoh (2006), Redetermination of the high-pressure modification of AlOOH from single-crystal synchrotron data, *Acta Crystallogr., Sect. E: Struct. Rep. Online*, *62*(11), i216–i218.
Lakshtanov, D. L., C. B. Vanpeteghem, J. M. Jackson, J. D. Bass, G. Shen, V. B. Prakapenka, K. Litasov, and E. Ohtani (2005), The equation of state of Al, H-bearing SiO_2 stishovite to 58 GPa, *Phys. Chem. Miner.*, *32*(7), 466–470.
Lakshtanov, D. L., et al. (2007), The post-stishovite phase transition in hydrous alumina-bearing SiO_2 in the lower mantle of the Earth, *Proc. Natl. Acad. Sci. U.S.A.*, *104*(34), 13,588–13,590.
Larson, A. C., and R. B. Von Dreele (1988), *Generalized Structure Analysis System*, Univ. of California, Berkeley.
Le Stunff, Y., C. W. Wicks Jr., and B. Romanowicz (1995), P'P'precursors under Africa: Evidence for mid-mantle reflectors, *Science*, *270*(5233), 74–74.
Leinenweber, K. D., J. A. Tyburczy, T. G. Sharp, E. Soignard, T. Diedrich, W. B. Petuskey, Y. Wang, and J. L. Mosenfelder (2012), Cell assemblies for reproducible multi-anvil experiments (the COMPRES assemblies), *Am. Mineral.*, *97*(2–3), 353–368.
Litasov, K. D., H. Kagi, A. Shatskiy, E. Ohtani, D. L. Lakshtanov, J. D. Bass, and E. Ito (2007), High hydrogen solubility in Al-rich stishovite and water transport in the lower mantle, *Earth Planet. Sci. Lett.*, *262*(3), 620–634.
Nishi, M., T. Irifune, J. Tsuchiya, Y. Tange, Y. Nishihara, K. Fujino, and Y. Higo (2014), Stability of hydrous silicate at high pressures and water transport to the deep lower mantle, *Nat. Geosci.*, *7*(3), 224–227.
Nisr, C., S.-H. Shim, K. Leinenweber, and A. Chizmeshya (2017), Raman spectroscopy of water-rich stishovite and dense high-pressure silica up to 55 GPa, *Am. Mineral.*, doi:10.2138/am-2017-5944, in press.
Niu, F., H. Kawakatsu, and Y. Fukao (2003), Seismic evidence for a chemical heterogeneity in the midmantle: A strong and slightly dipping seismic reflector beneath the Mariana subduction zone, *J. Geophys. Res.*, *108*(B9), 2419, doi:10.1029/2002JB002384.
Ohira, I., E. Ohtani, T. Sakai, T. Sakamaki, and M. Miyahara (2014), N. Hirao, Y. Ohishi, and M. Nishijima, Stability of a hydrous δ-phase, $AlOOH-MgSiO_2(OH)_2$, and a mechanism for water transport into the base of lower mantle, *Earth Planet. Sci. Lett.*, *401*, 12–17.
Ohtani, E., Y. Amaike, S. Kamada, T. Sakamaki, and N. Hirao (2014), Stability of hydrous phase H $MgSiO_4H_2$ under lower mantle conditions, *Geophys. Res. Lett.*, *41*, 8283–8287, doi:10.1002/2014GL061690.
Panero, W. R., L. R. Benedetti, and R. Jeanloz (2003), Transport of water into the lower mantle: Role of stishovite, *J. Geophys. Res.*, *108*(B1), 2039, doi:10.1029/2002JB002053.
Panero, W. R., J. S. Pigott, D. M. Reaman, J. E. Kabbes, and Z. Liu (2015), Dry (Mg, Fe) SiO_3 perovskite in the Earth's lower mantle, *J. Geophys. Res. Solid Earth*, *120*, 894–908, doi:10.1002/2014JB011397.

Pawley, A. R., P. F. McMillan, and J. R. Holloway (1993), Hydrogen in stishovite, with implications for mantle water content, *Science*, *261*, 1024–1024.

Prescher, C., and V. B. Prakapenka (2015), DIOPTAS: A program for reduction of two-dimensional X-ray diffraction data and data exploration, *High Pressure Res.*, *35*(3), 223–230.

Ricolleau, A., J.-p. Perrillat, G. Fiquet, I. Daniel, J. Matas, A. Addad, N. Menguy, H. Cardon, M. Mezouar, and N. Guignot (2010), Phase relations and equation of state of a natural MORB: Implications for the density profile of subducted oceanic crust in the Earth's lower mantle, *J. Geophys. Res.*, *115*, B08202, doi:10.1029/2009JB006709.

Rivers, M., V. B. Prakapenka, A. Kubo, C. Pullins, C. M. Holl, and S. D. Jacobsen (2008), The COMPRES/GSECARS gas-loading system for diamond anvil cells at the Advanced Photon Source, *High Pressure Res.*, *28*(3), 273–292.

Rossman, G. (1996), Studies of OH in nominally anhydrous minerals, *Phys. Chem. Miner.*, *23*(4–5), 299–304.

Sano-Furukawa, A., H. Kagi, T. Nagai, S. Nakano, S. Fukura, D. Ushijima, R. Iizuka, E. Ohtani, and T. Yagi (2009), Change in compressibility of δ-AlOOH and δ-AlOOD at high pressure: A study of isotope effect and hydrogen-bond symmetrization, *Am. Mineral.*, *94*(8–9), 1255–1261.

Shieh, S. R., T. S. Duffy, and B. Li (2002), Strength and elasticity of SiO_2 across the stishovite–$CaCl_2$-type structural phase boundary, *Phys. Rev. Lett.*, *89*(25), 255–507.

Smyth, J. R., R. J. Swope, and A. R. Pawley (1995), H in rutile-type compounds: II. Crystal chemistry of Al substitution in H-bearing stishovite, *Am. Mineral.*, *80*(5–6), 454–456.

Spektor, K., J. Nylen, E. Stoyanov, A. Navrotsky, R. L. Hervig, K. Leinenweber, G. P. Holland, and U. Häussermann (2011), Ultrahydrous stishovite from high-pressure hydrothermal treatment of SiO_2, *Proc. Natl. Acad. Sci. U.S.A.*, *108*(52), 20,918–20,922.

Spektor, K., J. Nylén, R. Mathew, M. Edén, E. Stoyanov, A. Navrotsky, K. Leinenweber, and U. Häussermann (2016), Formation of hydrous stishovite from coesite in high pressure hydrothermal environments, *Am. Mineral.*, *101*, 2514–2524.

Stishov, S., and S. Popova (1961), A new dense modification of silica, *Geokhimiya*, *10*, 837–841.

Suzuki, A., E. Ohtani, and T. Kamada (2000), A new hydrous phase δ-AlOOH synthesized at 21 GPa and 1000°C, *Phys. Chem. Miner.*, *27*(10), 689–693.

Umemoto, K., K. Kawamura, K. Hirose, and R. M. Wentzcovitch (2016), Post-stishovite transition in hydrous aluminous SiO_2, *Phys. Earth Planet. Inter.*, *255*, 18–26.

Vinnik, L., M. Kato, and H. Kawakatsu (2001), Search for seismic discontinuities in the lower mantle, *Geophys. J. Int.*, *147*(1), 41–56.

Walter, M., S. Kohn, D. Araujo, G. Bulanova, C. Smith, E. Gaillou, J. Wang, A. Steele, and S. Shirey (2011), Deep mantle cycling of oceanic crust: Evidence from diamonds and their mineral inclusions, *Science*, *334*(6052), 54–57.

Erratum

In the originally published version of this article, the values of the unit cell parameter c(Å) and the unit cell volume V_0(Å^3) for anhydrous stishovite samples in Table 2 were incorrect. The table has since been corrected and this version may be considered the authoritative version of record.